VIP Chirality Very Important Paper

International Edition: DOI: 10.1002/anie.201507918
German Edition: DOI: 10.1002/ange.201507918

Remote Control of the Planar Chirality in Peptide-Bound Metallomacrocycles and Dynamic-to-Static Planar Chirality Control Triggered by Solvent-Induced 3_{10}-to-α-Helix Transitions

Fumihiko Mamiya, Naoki Ousaka, and Eiji Yashima**

Abstract: *The dynamic planar chirality in a peptide-bound Ni^{II}-salphen-based macrocycle can be remotely controlled. First, a right-handed (P)-3_{10}-helix is induced in the dynamic helical oligopeptides by a chiral amino acid residue far from the macrocyclic framework. The induced planar chirality remains dynamic in chloroform and acetonitrile, but is almost completely locked in fluoroalcohols as a result of the solvent-induced transition of the peptide chains from a 3_{10}-helix to a wider α-helix, which freezes the rotation of the pendant peptide units around the macrocycle.*

Long-range communication is ubiquitous in biological systems, for example in allosteric enzymes.[1] Such long-range information transfer has been successfully achieved in artificial helical systems based on the chiral domino effect,[2] through which an excess of either a right- (*P*) or left-handed (*M*) helical conformation can be induced in dynamic helical polymers and oligomers including peptides that are composed of achiral components by covalently or noncovalently introducing chiral residues at the chain ends. Taking advantage of this unique chiral domino effect, we recently succeeded in the multistep remote control of the dynamic metal-centered chirality (Δ or Λ) of complexes coordinated by 2,2′-bipyridine (bpy) ligands bearing dynamic helical oligopeptides.[3] We anticipated that this multistep remote-control strategy based on the chiral domino effect would be applicable to control other types of complex supramolecular chirality,[4] such as the planar chirality of macrocycles.[5]

To this end, we synthesized novel dynamic peptide-bound Ni^{II}-salphen-based macrocycles[6] (Figure 1 a) in which the planar chirality results from the relative orientations of the peptide-bound phenylene units, which can rotate around the macrocyclic plane via the peptide chains passing through the inside of the macrocyclic cavity, thus producing four interconvertible diastereomers [(p*S*,p*S*,p*S*), (p*R*,p*S*,p*S*), (p*R*,p*R*,p*S*), and (p*R*,p*R*,p*R*)].

Two dynamic peptides with the sequence $(Ac_6c)_n$-L-Val-Aib-OTg ($n = 4$ and 6)[7] were employed as pendants of the macrocycles based on a previous study[3] (Figure 1 a). The peptide-bound Ni^{II}-salphen-based macrocycles were prepared by the reactions of the peptide-bound disalicylaldehydes $\mathbf{1}_{6mer}$ and $\mathbf{2}_{8mer}$ with *ortho*-phenylenediamine in the presence of nickel(II) acetate, producing the desired metallomacrocycles $\mathbf{3}_{6mer}$ and $\mathbf{4}_{8mer}$ (Figure 1 a), respectively, in high yields (92–97 %).[9]

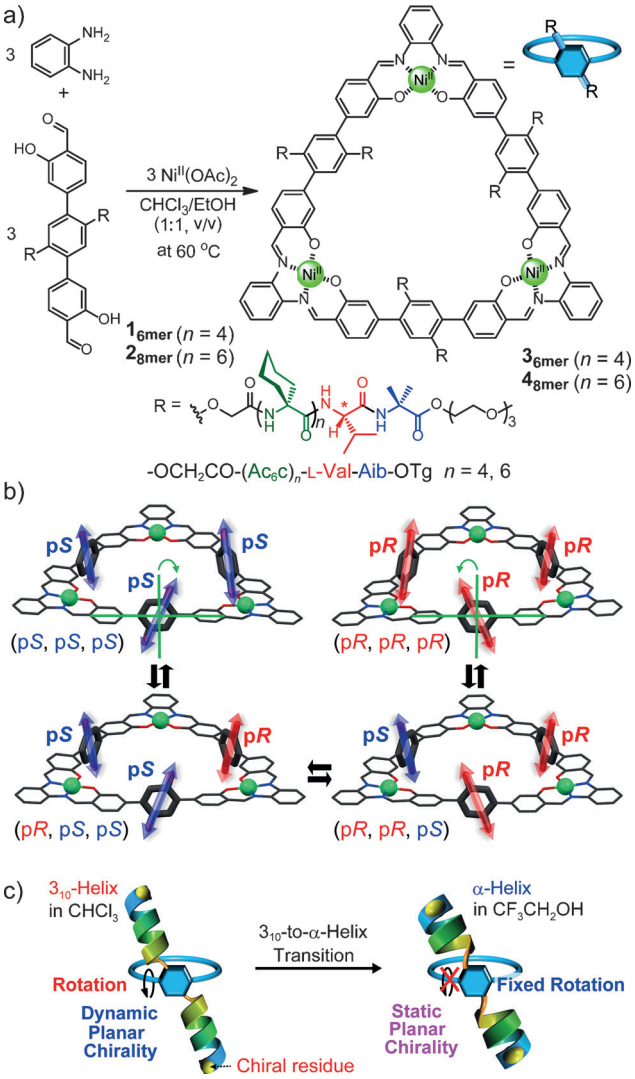

Figure 1. a) Chemical structures of $\mathbf{1}_{6mer}$–$\mathbf{4}_{8mer}$ and synthesis of the planar-chiral Ni^{II}-salphen-based macrocycles $\mathbf{3}_{6mer}$ and $\mathbf{4}_{8mer}$. b) Interconversion between four diastereomers of the planar-chiral Ni^{II}-salphen-based macrocycle ((p*S*,p*S*,p*S*), (p*R*,p*S*,p*S*), (p*R*,p*R*,p*S*), and (p*R*,p*R*,p*R*)). The peptide chains are omitted for clarity. c) Dynamic-to-static planar chirality in the macrocycle, triggered by a solvent-induced 3_{10}-to-α-helix transition.

[*] F. Mamiya, Dr. N. Ousaka, Prof. Dr. E. Yashima
Department of Molecular Design and Engineering
Graduate School of Engineering
Nagoya University
Chikusa-ku, Nagoya 464-8603 (Japan)
E-mail: ousaka@apchem.nagoya-u.ac.jp
yashima@apchem.nagoya-u.ac.jp
Homepage: http://helix.mol.nagoya-u.ac.jp/

Supporting information for this article is available on the WWW under http://dx.doi.org/10.1002/anie.201507918.

The IR absorption, ^{1}H NMR, and circular dichroism (CD) spectra of the Boc-protected model peptides (Boc-$(Ac_6c)_n$-L-Val-Aib-OTg; $n = 4$ and 6; Boc = *tert*-butoxycarbonyl) or the ligands $\mathbf{1}_{6mer}$ and $\mathbf{2}_{8mer}$ in solvents of various polarity, including $CHCl_3$, CH_3CN, and fluoroalcohols, such as 2,2,2-trifluoroethanol (TFE) and 1,1,1,3,3,3-hexafluoroisopropanol (HFIP), revealed that they preferentially adopted a (*P*)-3_{10}-helix[8e] in $CHCl_3$ and CH_3CN (Supporting Information, Figure S4–S7), but a (*P*)-α-helix in TFE and HFIP (Figure S7).[10]

The CD spectra of the macrocycles $\mathbf{3}_{6mer}$ and $\mathbf{4}_{8mer}$ in $CDCl_3$ are shown in Figure 2a. Interestingly, the macrocycle

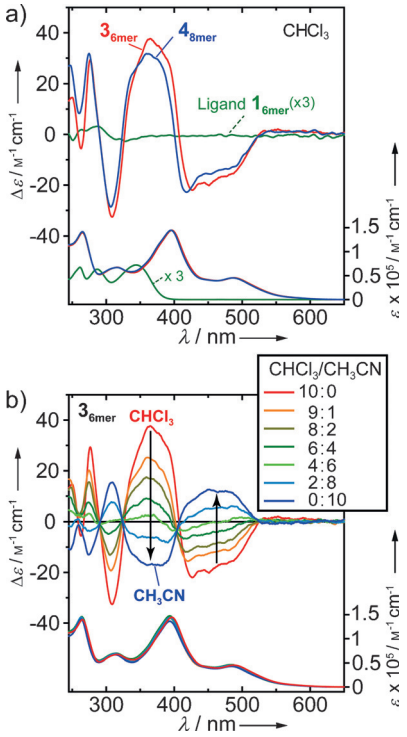

Figure 2. a) CD (top) and absorption (bottom) spectra of $\mathbf{3}_{6mer}$ (red) and $\mathbf{4}_{8mer}$ (blue) in $CHCl_3$ at the thermodynamic equilibrium state at 25 °C: [macrocycle] = 1.0×10^{-5} M. CD and absorption spectra of $\mathbf{1}_{6mer}$ (green) in $CHCl_3$ at 25 °C are also shown: $[\mathbf{1}_{6mer}] = 3.0\times10^{-5}$ M. b) CD (top) and absorption (bottom) spectra of $\mathbf{3}_{6mer}$ in various $CHCl_3$/CH_3CN mixtures (v/v) at the thermodynamic equilibrium state at 25 °C: $[\mathbf{3}_{6mer}] = 1.0\times10^{-5}$ M.

$\mathbf{4}_{8mer}$, which has longer octapeptide chains and a 1.5 times longer distance between the L-Val residue and the macrocyclic moiety than $\mathbf{3}_{6mer}$, exhibited a nearly identical Cotton effect even at the metal-to-ligand charge transfer band around 500 nm, whereas ligand $\mathbf{1}_{6mer}$ did not show an apparent CD signal in this region. These results indicate that chiral information at the terminal L-Val residue is transferred through the long achiral peptide chains with almost no loss of chiral information to induce the (*P*)-3_{10}-helix, which further induces an excess of either p*R* or p*S* planar chirality around each of the three phenylene units despite the chiral center (L-Val) being far from the macrocyclic framework.

The ^{1}H NMR spectra of $\mathbf{3}_{6mer}$ and $\mathbf{4}_{8mer}$ in $CDCl_3$ were then measured to gain insight into the diastereomeric ratios, but they were rather complicated owing to the mixture of diastereomers slowly interconverting on the NMR time scale (Figure S8).[11] However, unlike the other resonances, the proton signals of the terminal methoxy groups of $\mathbf{3}_{6mer}$ were well separated (Figures S8a and S9). Given the structural symmetry of the four diastereomers (Figure 1b), the D_{3h} symmetric [(p*R*,p*R*,p*R*) and (p*S*,p*S*,p*S*)] and less symmetric [(p*R*,p*R*,p*S*) and (p*S*,p*S*,p*R*)] diastereomers should give one and three sets of ^{1}H NMR signals, respectively, resulting in a total of eight sets of signals. Although these methoxy peaks partially overlapped (Figure S9), deconvolution of the methoxy peak clusters around 3.38–3.34 ppm allowed us to estimate the diastereomeric ratio in $CDCl_3$ at 25 °C: (p*R*,p*R*,p*R*)/(p*R*,p*R*,p*S*)/(p*R*,p*S*,p*S*)/(p*S*,p*S*,p*S*) or (p*S*,p*S*,p*S*)/(p*R*,p*S*,p*S*)/(p*R*,p*R*,p*S*)/(p*R*,p*R*,p*R*) ≈ 63:23:9:5 and p*R*/p*S* (or p*S*/p*R*) ≈ 81:19.[12]

Interestingly, the CD spectral pattern and intensity of $\mathbf{3}_{6mer}$ dramatically changed in mixtures of $CDCl_3$ and CD_3CN (Figure 2b); an increase in the CH_3CN content initially resulted in a decrease of the CD intensity, followed by inversion of the Cotton effect signs at high CH_3CN contents, accompanied by a negligible change in their absorption spectra; these results imply a solvent-dependent inversion of the planar chirality of $\mathbf{3}_{6mer}$ (p*R*/p*S* inversion).[13] The macrocycle $\mathbf{4}_{8mer}$, however, did not show such an inversion of the CD spectrum even in a $CHCl_3$/CH_3CN mixture (1:9, v/v), but exhibited weak CD (Figure S10). The reasons for the CH_3CN-induced CD spectral changes observed for $\mathbf{3}_{6mer}$ and $\mathbf{4}_{8mer}$ are not clear, but a possible helix-sense inversion of the peptide chains in the $CDCl_3$ and CD_3CN mixtures could be excluded.[3a]

The solvent-induced CD intensity changes of $\mathbf{3}_{6mer}$ and $\mathbf{4}_{8mer}$ were slow enough to be monitored by CD spectroscopy, and the kinetics of the planar chirality inversion, namely, the rotation rate of the phenylene units around the macrocyclic framework (Figure 3a), were estimated by diluting a $CHCl_3$ solution of $\mathbf{3}_{6mer}$ or $\mathbf{4}_{8mer}$ with CH_3CN ($CHCl_3$/CH_3CN = 1:9, v/v; method I, Figure 3b) and further solvent exchange from the $CHCl_3$/CH_3CN mixture to pure $CHCl_3$ (method II, Figure 3c). The CD inversion process of $\mathbf{3}_{6mer}$ was too fast to be followed in a $CHCl_3$/CH_3CN mixture (Figures 3b and S11a), whereas a $CHCl_3$ solution of $\mathbf{3}_{6mer}$, prepared from the $CHCl_3$/CH_3CN mixture (II), showed slow changes in CD (Figure 3c), and its CD spectrum finally recovered its original appearance in $CHCl_3$ (Figure S11b). Thus, the apparent rate constant (k in s^{-1}) for the interconversion between p*R* and p*S* for $\mathbf{3}_{6mer}$ was estimated to be 1.91×10^{-2} in $CHCl_3$ at 25 °C by a linear regression analysis (Table S2). On the other hand, the k values of $\mathbf{4}_{8mer}$ in $CHCl_3$ and in a $CHCl_3$/CH_3CN mixture (1:9, v/v) at 25 °C were 1.33×10^{-4} and 4.27×10^{-3}, respectively, which were much lower than those of $\mathbf{3}_{6mer}$ (Figures 3b,c and S11c,d and Table S2) owing to the longer 3_{10}-helical peptide chains of $\mathbf{4}_{8mer}$ (ca. 1.8 nm, Figure 4b)[14] compared to those of $\mathbf{3}_{6mer}$ (ca. 1.5 nm; Figure 4a).[15] Importantly, these helix lengths exceed the inner diameter of the rigid macrocycle (ca. 1.2 nm) estimated from the energy-minimized structure of $\mathbf{3}_{6mer}$ (Figure 4a), suggesting that rotation of the phenylene units may be difficult or seemingly impossible. However, this discrepancy could be solved by taking a helix reversal[2g] into

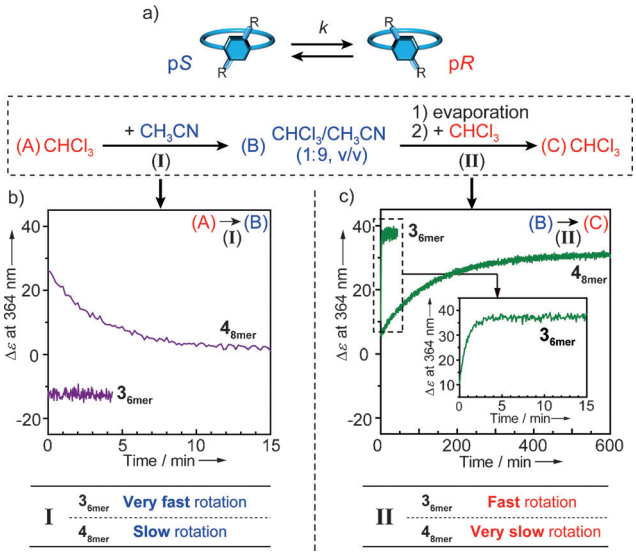

Figure 3. a) p*R*/p*S* chirality interconversion of the salphen-based macrocycle. Only one of the three phenylene rings is shown for clarity. b, c) Time-dependent CD intensity changes at 364 nm for $\mathbf{3}_{6mer}$ and $\mathbf{4}_{8mer}$ at 25 °C: [macrocycle] = 1.0–0.97 × 10^{-5} M. These measurements were performed according to the following procedures: The initial $CHCl_3$ solution of the macrocycle (A) was diluted tenfold with CH_3CN ($CHCl_3/CH_3CN$ = 1:9, v/v) at 25 °C (B; method I). After reaching an equilibrium state, the $CHCl_3/CH_3CN$ (1:9, v/v) mixed solution of the macrocycle was evaporated in a stream of N_2. The residue was then redissolved in $CHCl_3$ at 25 °C (C; method II). Solvent-dependent CD spectral changes are shown in Figure S11.

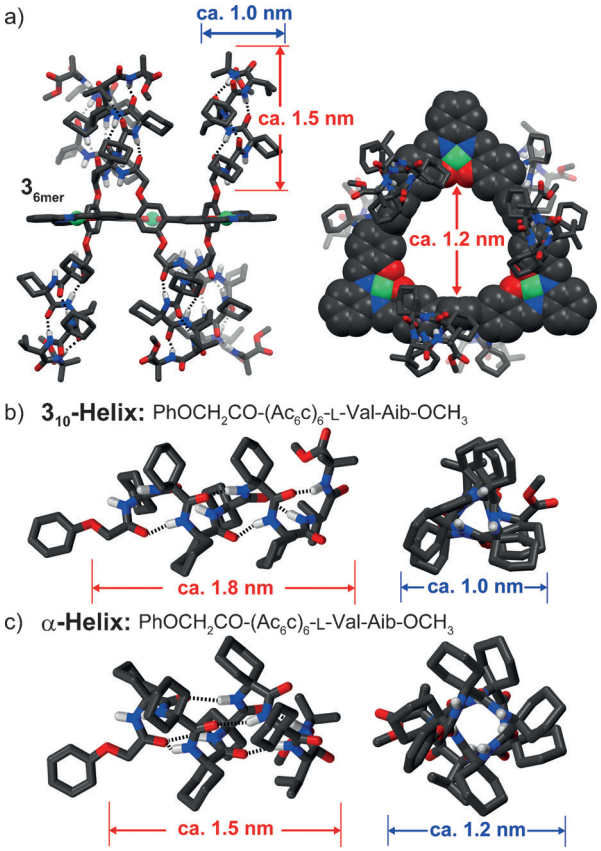

Figure 4. Side (left) and top (right) views of the energy-minimized (*P*)-3_{10}-helical peptide-bound macrocyclic structure of (p*R*,p*R*,p*R*)-$\mathbf{3}_{6mer}$ (a) and the energy-minimized (*P*)-3_{10}-helical (b) and (*P*)-α-helical (c) conformations of the octapeptide $PhOCH_2CO$-$(Ac_6c)_6$-L-Val-Aib-OCH_3. Hydrogen atoms except for the amide protons are omitted for clarity. Black dotted lines represent intramolecular hydrogen bonds. The C-terminal OTg groups were replaced with OCH_3 groups to simplify the calculation.

account that occurs at the achiral peptide segment through a bent-shaped conformational change along the entire single peptide chain,[16] thereby enabling the rotation of the peptide-bound phenylene units around the macrocycle.[17]

As described above, $\mathbf{4}_{8mer}$ showed weak CD in a $CHCl_3/CH_3CN$ mixture (1:9, v/v) at 25 °C (Figure S10), suggesting almost no preferred handed planar chirality, so that the kinetics of the flip-flop motion (epimerization with respect to the planar chirality) of the peptide-bound phenylene units can be estimated. The pseudo-first-order rate constants (k_{flip}, s^{-1}) estimated at different temperatures provide the following thermodynamic parameters by Arrhenius and Eyring plots of the data (Figure S12): $E_a = 117\ kJ\,mol^{-1}$, $\Delta G^{\ddagger}_{20} = 88.7\ kJ\,mol^{-1}$, $\Delta H^{\ddagger} = 115\ kJ\,mol^{-1}$, and $\Delta S^{\ddagger} = 91.2\ J\,mol^{-1}\,K^{-1}$. A large positive entropy of activation suggests that the transition state of the p*R*/p*S* inversion process is based on a highly distorted macrocyclic structure together with a distorted helical peptide structure caused by the helix reversal.

We next investigated whether the dynamic planar chirality of $\mathbf{3}_{6mer}$ and $\mathbf{4}_{8mer}$ could be regulated by the solvent-induced 3_{10}-to-α-helix transition of the pendant peptides using fluoroalcohols. Interestingly, the CD intensities at 349 nm of $\mathbf{3}_{6mer}$ in TFE, prepared either from a $CHCl_3$ solution (method III) and from a $CHCl_3/CH_3CN$ solution (1:9, v/v; method IV) through solvent exchange, very slowly changed as compared to those in $CHCl_3/CH_3CN$ (1:9, v/v) and $CHCl_3$ (Figure 3) and finally reached a plateau value at thermodynamic equilibrium in TFE (Figures 5a and S13a,c, and d);[18] the p*R*/p*S* interconversion of $\mathbf{3}_{6mer}$ was much slower in TFE than in $CHCl_3$ (by a factor of 62; Table S2). When HFIP was used instead of TFE, the CD intensity of $\mathbf{3}_{6mer}$ changed more slowly (Figure S14c), with a decrease in the *k* value from 3×10^{-4} (TFE) to 2.55×10^{-5} (HFIP; Table S2), and the resulting CD intensity was stronger than in TFE (Figures S13a and S14a). This is most likely due to an increase in the (*P*)-α-helix content in HFIP compared to that in TFE (Figure S7). As a consequence, the p*R*/p*S* interconversion of $\mathbf{3}_{6mer}$ in $CHCl_3$ was remarkably slowed down in HFIP by a factor of approximately 750 because of the solvent-induced 3_{10}-to-α-helix transition.

The kinetics of the interconversion of $\mathbf{4}_{8mer}$ in TFE and HFIP were also examined. Surprisingly, the CD intensities at 349 nm of $\mathbf{4}_{8mer}$ in TFE and HFIP prepared from a $CHCl_3/CH_3CN$ mixture (1:9, v/v; method IV) and $CHCl_3$ (method III) remained unchanged even after 450 min (Figures 5a, S13b–e, and S14b–e), indicating that the dynamic p*R*/p*S* interconversion of $\mathbf{4}_{8mer}$ was locked at 25 °C.[19] As a result, the interconvertible dynamic planar chirality of the macrocycle $\mathbf{4}_{8mer}$ was completely trapped kinetically, while maintaining its original handedness (p*R* or p*S* rich) in $CHCl_3$ and $CHCl_3/$

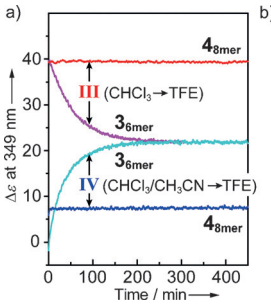

b)

Solvent	Helix type	3_{8mer}	4_{8mer}
$CHCl_3$	3_{10}-helix	Fast rotation	Very slow rotation
(III)↓ TFE or HFIP (IV)↑	α-helix	Very slow rotation	Fixed rotation
$CHCl_3$/CH_3CN (1:9)	3_{10}-helix	Very fast rotation	Slow rotation

Figure 5. a) Time-dependent changes of the CD intensity at 349 nm for $\mathbf{3}_{6mer}$ and $\mathbf{4}_{8mer}$ in TFE at 25 °C, after replacing $CHCl_3$ (method III) and a $CHCl_3$/CH_3CN mixture (1:9, v/v; method IV) with TFE. [macrocycle] = 1.0×10^{-5} M. Solvent replacement was carried out by evaporation of the first solvents, followed by redissolution in TFE. Solvent-dependent CD spectral changes are shown in Figure S13a, b. b) Summary of the solvent-induced control of dynamic planar chirality in metallomacrocycles resulting from the 3_{10}-to-α-helix conformational transition of the pendant peptides.

CH_3CN (1:9, v/v). This unprecedented dynamic-to-static conformational manipulation of the planar chirality of $\mathbf{4}_{8mer}$ results from the TFE- and HFIP-induced conformational transition of the pendant peptide chains of $\mathbf{4}_{8mer}$ from the narrower 3_{10}-helix (ca. 1.0 nm) to the wider α-helix (ca. 1.2 nm; Figure 4b,c) as supported by the inner diameter of the Ni^{II}-salphen-based macrocycle (ca. 1.2 nm; Figure 4a), which is very close to the α-helix width. However, the helix length of the α-helix (ca. 1.5 nm) of the octapeptide is shorter than that of the corresponding 3_{10}-helix (ca. 1.8 nm; Figure 4b,c). Therefore, the width of the pendant helix, rather than its length, is crucial for suppressing the p*R*/p*S* interconversion in this system.

In summary, we have described an unprecedented domino-type remote control and further fixation of the planar chirality of macrocycles as a result of a solvent-induced 3_{10}- to α-helix transition of the peptide chains, which freezes the rotation of the peptide-bound phenylene rings around the macrocycle because of the increased helix width. These findings may provide a rational design strategy not only for novel chiral macrocyclic hosts for the enantioselective inclusion of large chiral guest molecules, but also for developing macrocycle-based ion channels that make use of 3_{10}-to-α-helix transitions.

Acknowledgements

This work was supported in part by a Grant-in-Aid for Scientific Research (S) (25220804 to E.Y.) and a Grant-in-Aid for Young Scientists (B) (26810047 to N.O.) from the Japan Society for the Promotion of Science (JSPS), and by the Nanotechnology Platform Program (Molecule and Material Synthesis) of the Ministry of Education, Culture, Sports, Science and Technology, Japan.

Keywords: chirality · macrocycles · peptides · self-assembly · supramolecular chemistry

How to cite: *Angew. Chem. Int. Ed.* **2015**, *54*, 14442–14446
Angew. Chem. **2015**, *127*, 14650–14654

[1] a) J. Monod, J. Wyman, J.-P. Changeux, *J. Mol. Biol.* **1965**, *12*, 88–118; b) Z. Bu, D. J. E. Callaway in *Advances in Protein Chemistry and Structural Biology, Vol. 83* (Ed.: D. Rossen), Academic Press, San Diego, **2011**, pp. 163–221.

[2] For examples of domino-type chiral information transfer along achiral peptide backbones, see: a) Y. Inai, K. Tagawa, A. Takasu, T. Hirabayashi, T. Oshikawa, M. Yamashita, *J. Am. Chem. Soc.* **2000**, *122*, 11731–11732; b) Y. Inai, Y. Ishida, K. Tagawa, A. Takasu, T. Hirabayashi, *J. Am. Chem. Soc.* **2002**, *124*, 2466–2473; c) J.-P. Mazaleyrat, K. Wright, A. Gaucher, N. Toulemonde, M. Wakselman, S. Oancea, C. Peggion, F. Formaggio, V. Setnička, T. A. Keiderling, C. Toniolo, *J. Am. Chem. Soc.* **2004**, *126*, 12874–12879; d) J. Clayden, A. Castellanos, J. Solà, G. A. Morris, *Angew. Chem. Int. Ed.* **2009**, *48*, 5962–5965; *Angew. Chem.* **2009**, *121*, 6076–6079; e) B. A. F. Le Bailly, L. Byrne, V. Diemer, M. Foroozandeh, G. A. Morris, J. Clayden, *Chem. Sci.* **2015**, *6*, 2313–2322; for recent reviews on dynamic helical polymers and oligomers, see: f) D. J. Hill, M. J. Mio, R. B. Prince, T. S. Hughes, J. S. Moore, *Chem. Rev.* **2001**, *101*, 3893–4012; g) E. Yashima, K. Maeda, H. Iida, Y. Furusho, K. Nagai, *Chem. Rev.* **2009**, *109*, 6102–6211.

[3] a) N. Ousaka, Y. Takeyama, H. Iida, E. Yashima, *Nat. Chem.* **2011**, *3*, 856–861; b) N. Ousaka, Y. Takeyama, E. Yashima, *Chem. Eur. J.* **2013**, *19*, 4680–4685.

[4] For reviews, see: a) J. Crassous, *Chem. Soc. Rev.* **2009**, *38*, 830–845; b) A. M. Castilla, W. J. Ramsay, J. R. Nitschke, *Acc. Chem. Res.* **2014**, *47*, 2063–2073.

[5] For a review, see: a) R. Chakrabarty, P. S. Mukherjee, P. J. Stang, *Chem. Rev.* **2011**, *111*, 6810–6918; for planar-chiral pillar-[5]arenes, see: b) T. Ogoshi, S. Kanai, S. Fujinami, T.-a. Yamagishi, Y. Nakamoto, *J. Am. Chem. Soc.* **2008**, *130*, 5022–5023; c) T. Ogoshi, R. Shiga, T.-a. Yamagishi, Y. Nakamoto, *J. Org. Chem.* **2011**, *76*, 618–622; d) T. Ogoshi, T. Akutsu, D. Yamafuji, T. Aoki, T.-a. Yamagishi, *Angew. Chem. Int. Ed.* **2013**, *52*, 8111–8115; *Angew. Chem.* **2013**, *125*, 8269–8273.

[6] For reviews on metallosalphen- or metallosalen-based supramolecules, see: a) S. Akine, T. Nabeshima, *Dalton Trans.* **2009**, 10395–10408; b) C. J. Whiteoak, G. Salassa, A. W. Kleij, *Chem. Soc. Rev.* **2012**, *41*, 622–631.

[7] 1-Aminocyclohexane-1-carboxylic acid (Ac_6c)[8a–c] and α-aminoisobutyric acid (Aib)[8d,e] are known as strong helicogenic achiral amino acids; OTg = 2-(2-(2-methoxyethoxy)ethoxy)ethyl.

[8] a) P. K. C. Paul, M. Sukumar, R. Bardi, A. M. Piazzesi, G. Valle, C. Toniolo, P. Balaram, *J. Am. Chem. Soc.* **1986**, *108*, 6363–6370; b) V. Pavone, E. Benedetti, V. Barone, B. Di Blasio, F. Lelj, C. Pedone, A. Santini, M. Crisma, G. M. Bonora, C. Toniolo, *Macromolecules* **1988**, *21*, 2064–2070; c) M. Crisma, G. M. Bonora, C. Toniolo, A. Bavoso, E. Benedetti, B. Di Blasio, V. Pavone, C. Pedone, *Macromolecules* **1988**, *21*, 2071–2074; d) I. L. Karle, P. Balaram, *Biochemistry* **1990**, *29*, 6747–6756; e) C. Tonlolo, E. Benedetti, *Trends Biochem. Sci.* **1991**, *16*, 350–353.

[9] For the synthesis and characterization of the new peptide ($n = 6$), the ligands ($\mathbf{1}_{6mer}$ and $\mathbf{2}_{8mer}$), and the macrocycles ($\mathbf{3}_{6mer}$ and $\mathbf{4}_{8mer}$), see the Supporting Information.

[10] For examples of stimuli-responsive 3_{10}-to-α-helix transitions, see: a) G. Hungerford, M. Martinez-Insua, D. J. S. Birch, B. D. Moore, *Angew. Chem. Int. Ed. Engl.* **1996**, *35*, 326–329; *Angew. Chem.* **1996**, *108*, 356–359; b) T. S. Yokum, T. J. Gauthier, R. P. Hammer, M. L. McLaughlin, *J. Am. Chem. Soc.* **1997**, *119*, 1167–1168; c) P. Pengo, L. Pasquato, S. Moro, A. Brigo, F. Fogolari, Q. B. Broxterman, B. Kaptein, P. Scrimin, *Angew. Chem. Int. Ed.* **2003**, *42*, 3388–3392; *Angew. Chem.* **2003**, *115*, 3510–3514; d) K. Kitagawa, T. Morita, S. Kimura, *Angew. Chem. Int. Ed.* **2005**, *44*,

6330 – 6333; *Angew. Chem.* **2005**, *117*, 6488 – 6491; e) M. Crisma, M. Saviano, A. Moretto, Q. B. Broxterman, B. Kaptein, C. Toniolo, *J. Am. Chem. Soc.* **2007**, *129*, 15471 – 15473.

[11] This effect may be ascribed, at least in part, to the flexible -OCH_2- spacer between the pendant peptide chain and the phenylene unit, which may disturb the efficient stereochemical communication between the macrocyclic moiety and the (*P*)-3_{10}-helical peptides. A similar non-perfect diastereoselectivity has also been found in a pillar[5]arene bearing chiral substituents on both rims through the -OCH_2- spacer, and the diastereomeric ratio p*R*/p*S* (or p*S*/p*R*) was reported to be 56.7:43.3 under conditions similar to those in the present study ($CDCl_3$, 25 °C).[5c]

[12] The diastereomeric ratio of $\mathbf{4}_{\mathbf{8mer}}$ could not be determined by ^{1}H NMR spectroscopy even at low temperatures because of broadening of the signals, and attempts to separate the diastereomers by HPLC were unsuccessful. However, the diastereomeric ratio of $\mathbf{4}_{\mathbf{8mer}}$ seems to be similar to that of $\mathbf{3}_{\mathbf{6mer}}$ because their CD intensities and spectral patterns are almost identical.

[13] In accordance with the CD spectral changes, the ^{1}H NMR signals of the terminal methoxy protons of $\mathbf{3}_{\mathbf{6mer}}$ significantly changed when measured in $CDCl_3$ and CD_3CN mixtures, and the major peak assigned to the (p*R*,p*R*,p*R*) or (p*S*,p*S*,p*S*) diastereomer in $CDCl_3$ decreased in intensity as the amount of CD_3CN was increased; however, the diastereomeric ratios could not be estimated owing to significant signal overlap (Figure S9).

[14] The helix length was estimated by the energy-minimized structure of the corresponding peptide in $\mathbf{4}_{\mathbf{8mer}}$ (Figure 4b).

[15] Their helix widths are identical (ca. 1.0 nm; Figure 4a, b).

[16] For examples, see: a) A. Banerjee, S. R. Raghothama, I. L. Karle, P. Balaram, *Biopolymers* **1996**, *39*, 279 – 285; b) V. Nanda, W. F. DeGrado, *J. Am. Chem. Soc.* **2006**, *128*, 809 – 816.

[17] It has been reported that the efficiency of chiral information transmittance along an Aib-based achiral peptide chain decreases with an increase in the solvent polarity;[2d,e,3b] in other words, the frequency of the helical reversal likely increases with increasing solvent polarity. In fact, the *k* values of $\mathbf{3}_{\mathbf{6mer}}$ and $\mathbf{4}_{\mathbf{8mer}}$ at 25 °C are much higher in a mixed polar solvent ($CHCl_3$/CH_3CN = 1:9, v/v) than in the less polar $CHCl_3$ (Table S2).

[18] The domino-type chiral information transfer along the achiral peptide chain has been limited to dynamic 3_{10}-helical peptides composed of achiral amino acid residues.[2a–e] Therefore, we have demonstrated for the first time that such a domino-type chiral information transfer takes place along the dynamic α-helical peptide chain; see the text below.

[19] This means that the remotely stereocontrolled planar chirality is diastereomerically "memorized", although the pendant peptide chains possess the chiral residue. For recent examples of chiral memory effects, see: a) W. Zhang, W. Jin, T. Fukushima, N. Ishii, T. Aida, *J. Am. Chem. Soc.* **2013**, *135*, 114 – 117; b) A. M. Castilla, N. Ousaka, R. A. Bilbeisi, E. Valeri, T. K. Ronson, J. R. Nitschke, *J. Am. Chem. Soc.* **2013**, *135*, 17999 – 18006; c) K. Shimomura, T. Ikai, S. Kanoh, E. Yashima, K. Maeda, *Nat. Chem.* **2014**, *6*, 429 – 434.

Received: August 29, 2015
Published online: October 1, 2015

